RESEARCH ARTICLE

Downscaling of the Land Surface Temperature Data Obtained at four Different Dates in a Year Using the GWR Model: A Case Study in Antakya, Turkey

Ahmet Irvem[1] · Mustafa Ozbuldu[1]

Abstract

Land surface temperature (LST) is a major factor that affects many biophysical processes in the land–atmosphere relationship. This factor is obtained from satellite images having different temporal and spatial resolutions. This study applied the geographically weighted regression (GWR) model for four different dates representing each season a year to improve the LST images obtained in coarse resolution. In this study, MODIS LST images that are available having fine temporal but coarse spatial resolution were modeled using NDBI and NDVI indices, and their spatial resolution is improved. In addition, LANDSAT 8 images were used as reference images to evaluate the accuracy of the images obtained from the models. Results of the GWR model have been evaluated by comparing it statistically with TsHARP and DisTradother commonly used methods. As a result of the comparison by using the average of four dates outputs, the GWR model ($R^2 = 0.73$, RMSE = 0.78) was more successful than the TsHARP ($R^2 = 0.56$, RMSE = 1.00) and DisTrad ($R^2 = 0.49$, RMSE = 1.09) methods. The most successful downscaling performance in the GWR model was obtained in the spring season (RSR = 0.48). According to these findings, the GWR model can be used for downscaling LST images in urban areas. However, before applying this algorithm to scenarios outside of urban areas, it is recommended to use the required parameters and optimize their combinations.

Keywords Geographically weighted regression · TsHARP · DisTrad · LST · Downscaling

Introduction

Land surface temperature (LST) is a critical parameter that affects many biophysical processes in the land–atmosphere relationship derived from solar radiation (Khan et al. 2021). LST is used in studies such as determining the amount of evapotranspiration (Anderson et al., 2012), hydrological cycle (Sun et al., 2007), climate change assessment (Wu et al., 2015a, 2015b), estimating the amount of radiation (Jiao et al., 2015), modeling the maximum-minimum temperature difference (Duan et al., 2017), ph enology of vegetation (Badeck et al., 2004), and monitoring the urban heat island (Caihua et al., 2011). LST images can be obtained by satellite having thermal sensors such as MODIS and LANDSAT 8 with different spatial and temporal resolutions. One of the biggest problems of currently used satellite thermal sensors is that they cannot have both high temporal and high spatial resolution at the same time due to technical and financial constraints (Mukherjee et al. 2015). In particular, MODIS LST can be obtained daily for an observed area. However, LST images are obtained at a coarse resolution (1000 m). Therefore, it is considered that the improvement in the spatial resolution of MODIS LST data is significant for many applications with high-resolution demands, both spatially and temporally (Peng et al., 2019; Yang et al., 2011). For this reason, researchers tend to find effective and low-cost methods that can be a solution to this problem. The most concentrated research on this subject has been applying downscaling methods to LST images in recent years (Duan & Li, 2016; Wu et al., 2015a, 2015b).

✉ Ahmet Irvem
   airvem@mku.edu.tr

[1] Department of Biosystems Engineering, Hatay Mustafa
    Kemal University, Hatay, Turkey

LST reduction is the process of separating the mixed pixels of the coarse resolution LST image by matching the spatial details of high-resolution images from the same or different sensors (Peng et al., 2019). In recent years, different approaches have been proposed to reduce the coarse resolution of the land surface temperature images to the regional scale. These algorithms have generally been developed based on correlations between LST images and auxiliary biophysical parameters acquired at better spatial resolution. In these algorithms, digital elevation data, land cover maps and reflectance images obtained from visible/ near-infrared wave bands are generally used as auxiliary parameters (Hutengs and Vohland 2016). In general, vegetation indices are preferred as an auxiliary parameter in such models because of the high correlation between them and LST.

One of the most widely used statistical regression methods is the DisTrad method proposed by Kustas et al. (2003). This method is based on the assumption that the relationship between the normalized difference vegetation index (NDVI) and the LST is invariant to scale. Another widely used downscaling method is the TsHARP method (Agam et al., 2007). In this method, NDVI maps are used as auxiliary parameters to sharpen the land surface temperatures to the resolution of the VIS/NIR waveband. The main limitation of the TsHARP algorithm is the relationship between NDVI and LTS is not unique, which results in a wide range of LSTs for a given value of NDVI (Bindhu et al., 2013; Duan & Li, 2016; Merlin et al., 2010). However, vegetation index-based downscaling models assume that regional-scale LST variability is dependent on regional vegetation. This situation can cause significant errors in the spatial LST distribution by causing changes in the amount of solar radiation in heterogeneous regions where regional differences in the region's topography and albedo exist (Dominguez et al., 2011; Hais & Kucera, 2009; Jeganathan et al., 2011). Therefore, in recent studies, alternative methods have been developed to the TsHARP method, taking into account the effect of photosynthetic and non-photosynthetic active vegetation within the spatial variability of LST (Peng et al., 2019). These methods both use various auxiliary parameters for downscaling the LST and use a geographic model that considers the spatial stability between these parameters and the LST. Yang et al. (2010) aimed to establish a regressive relationship between the LST and multiple factors, assuming that a single estimator cannot fully reflect the difference in LST in different land covers. The downscaling results showed that this algorithm gives better results than the traditional approach. Duan et al. (2016) used GWR as the LST downscaling algorithm. As a result, they obtained better results than the commonly used TsHARP algorithm. Peng et al. (2019) developed a geographic flywheel-weighted regression (GWR) model

for the spatial reduction of MODIS LST data from 1000 to 100 m. The results showed that the GWR algorithm performs better with lower RMSE than the traditional method. Wang et al. (2021) proposed a geographically weighted model to reduce the spatial resolution of MODIS LST from 1000 to 100 m, considering the spatial non-stationarity and obtained good downscaling results.

The main goal of this study is to use the GWR downscaling model to improve the spatial resolution of MODIS LST images by using NDBI and NDVI indices and to apply the model for Antakya, Turkey. LANDSAT 8 images that have fine spatial resolutions were used as reference images to determine the usability of the images obtained from the GWR, TsHARP and DisTrad models. Results have been evaluated by comparing them statistically with models for four different dates.

Material and Methods

Study Area

In this study, Antakya city located in the province of Hatay in Turkey was chosen for the case study. The locations of the study areas having the false-color images generated from the LANDSAT-8 data are given in Fig. 1. The coordinates of the study area are 36° 03′ 05′′ E to 36° 13′ 52′′ E and 36° 18′ 13′′ N to 36° 07′ 41′′ N. According to the Köppen climate classification, it is located in the Mediterranean climate with warm winters and very hot and dry summers. The annual average temperature is approximately 18.6 °C, where the lowest and highest temperatures are − 11.8 and 44.6 °C, respectively. The average annual precipitation is approximately 1124.2 mm. Land use and land cover map was obtained from CORINE given in Fig. 2.

Datasets and Preprocessing

In this study, LANDSAT 8 raw reflectance data and MODIS LST data taken from four different dates were used. The acquisition dates of LANDSAT 8 and MODIS LST images are given in Table 1.

In this study, the MOD11 collection with a spatial resolution of 1000 m was used as the auxiliary data for LST downscaling. The MODIS LST data were downloaded from the NASA website (https://ladsweb.modaps.eosdis.nasa.gov/). ArcGIS-10.8 software was used to process the MODIS dataset, which has hdf file format. In addition, the projection of the data was converted to the UTM WGS 1984 projection. Finally, using the following Eq. 1, MODIS LST data (DN value) were converted from Kelvin to Celsius temperature (Alqasemi et al., 2020);
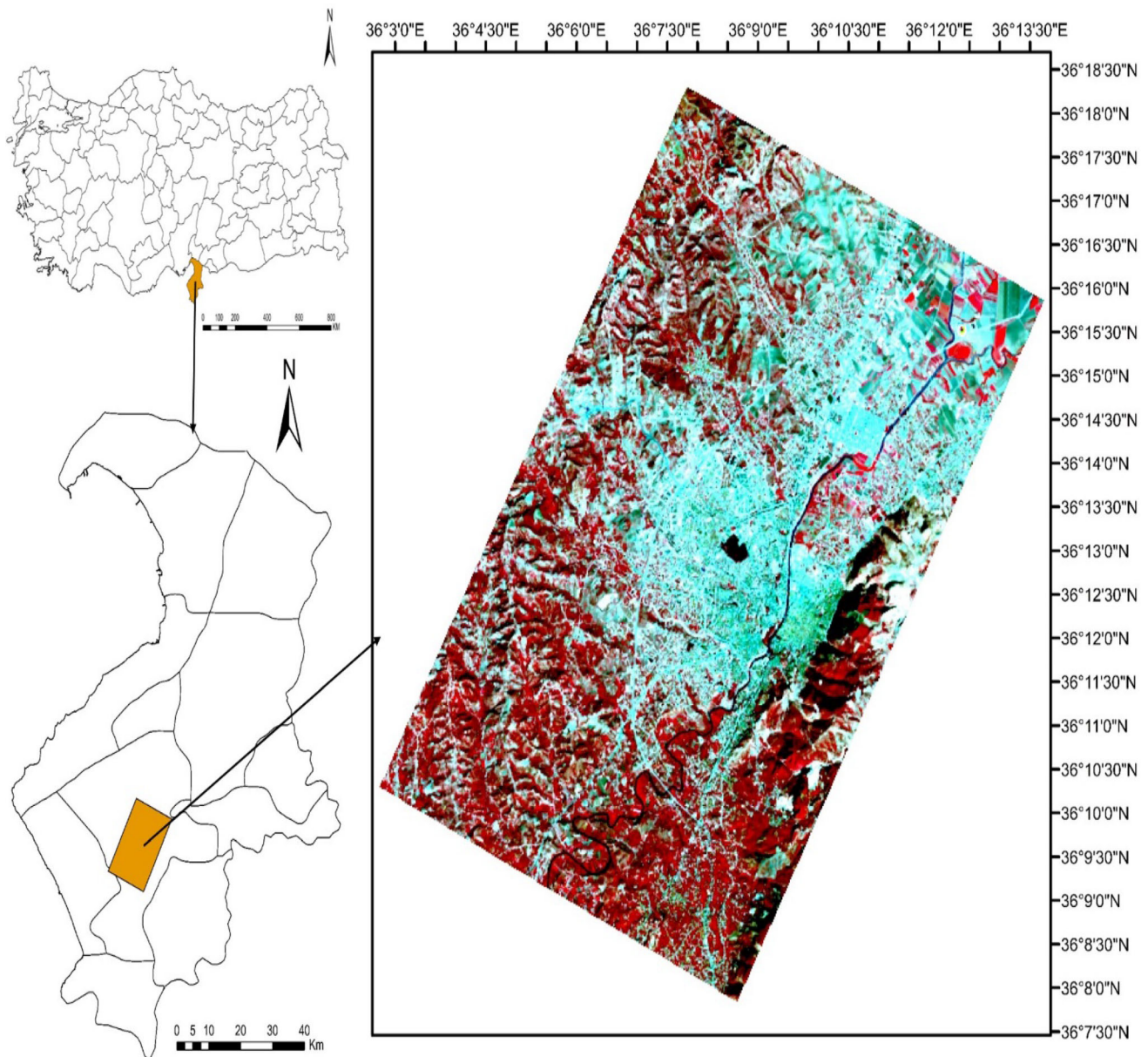
Fig. 1 Locations of the study areas with the false-color images generated from LANDSAT-8 data for 07.05.2021 (R: band 5, G: band 4, and B: band 3)

$$LST(°C) = (a * DN) - 273.15 \tag{1}$$

where LST is MODIS land surface temperature and a is the scaling factor (0.02) of the MODIS LST product.

LANDSAT 8 was launched by the National Aeronautics and Space Administration (NASA). Two sensors are carried by the LANDSAT 8 satellite, Thermal Infrared Sensor (TIRS) and OLI. The LANDSAT 8 data of this study was taken from the Earth Explorer data gateway (http://earth explorer.usgs.gov/). The downloaded LANDSAT 8 surface reflection data was obtained by processing with calibration and atmospheric correction modules from ENVI 5.3 software. In addition, the image-to-image module of ENVI 5.3

software was used for geometric correction between MODIS and LANDSAT 8 data. Feature points of LAND-SAT 8 data such as road and river were chosen as reference control points to correct MODIS images (Rawat et al., 2019; Zareie et al., 2016).

In this study, MODIS LST with 1000 km spatial resolution represents LST with coarse spatial resolution. LANDSAT 8 is used in two different stages in the down-scaling model. Firstly, LANDSAT 8 surface reflectance data with 30 m resolution was used to calculate auxiliary parameters Normalized Difference Vegetation Index (NDVI) and Normalized Difference Built-up Index (NDBI)
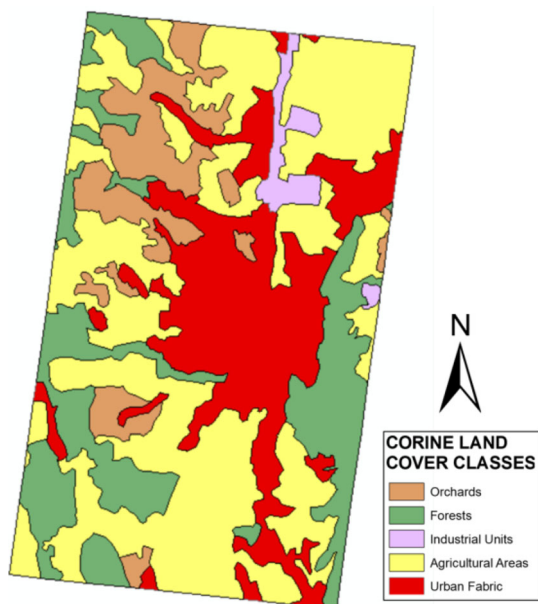
Fig. 2 Land use and land cover map for study area

to create the model given as Eq. 2 (Purevdorj et al., 1998) and Eq. 3 (Zha et al., 2003).

$$NDVI = \frac{R_{NIR} - R_{RED}}{R_{NIR} + R_{RED}} \tag{2}$$

$$NDBI = \frac{R_{SWIR1} - R_{NIR}}{R_{SWIR1} + R_{NIR}} \tag{3}$$

where R_{NIR}, R_{RED} and R_{SWIR1} are the reflectance values of the near-infrared band, red band and the first shortwave infrared band, respectively. The NDVI and NDBI data obtained were resampled to 100 m and 1000 m to establish the fine and coarse resolution model. Finally, LANDSAT 8 LST calculated with LANDSAT 8 data was used as reference data to validate the downscaling results. To calculate LANDSAT 8 LST, the Top of Atmospheric Spectral Radiance ($L\lambda$) was first calculated using Eq. 4.

$$L\lambda = M_L Q_{cal} + A_L - O_i \tag{4}$$

where M_L is the band-specific multiplicative rescaling factor (0.000342), Q_{cal} is the Band 10 image, A_L is the band-specific additive rescaling factor (0.1), and Oi is the correction for Band 10 (0.29) (Barsi et al., 2014). Second, the TIRS band data needs to be converted to brightness

temperature (BT). For this, thermal constants provided in the metadata file were used (Eq. 5).

$$BT = \frac{K_2}{\ln[(K_1/L\lambda) + 1]} - 273.15\Delta \tag{5}$$

where K_1 (1321.08) and K_2 (777.89) represent the band-specific thermal conversion constants (Avdan & Jovanovska, 2016). Existing vegetation is an important factor affecting the surface temperature. For this reason, NDVI is very important to obtain information about the general vegetation of the study area because vegetation rate can be calculated using NDVI (Eq. 6) (Song et al., 2017).

$$P_v = \left(\frac{NDVI - NDVI_{min}}{NDVI_{max} - NDVI_{min}} \right)^2 \tag{6}$$

In another step, the land surface emissivity (LSE) has to be calculated (Eq. 7) because LSE ($\varepsilon\lambda$) is the efficiency of transmitting thermal energy from the surface to the atmosphere.

$$\varepsilon\lambda = 0.004 \, P_v + 0.986 \tag{7}$$

The final step in calculating the LST is as given in Eq. 8.

$$LST = \frac{BT}{\{1 + [(\lambda BT/\rho) \ln \varepsilon\lambda]\}} \tag{8}$$

$$\rho = h\frac{c}{\sigma} = 1.438x \times 10^{-2} \text{m K} \tag{9}$$

where λ is the wavelength of emitted radiance (10.895), ρ is Planck's constant (6.626×10^{-34} J s), c is the velocity of light (2.998×108 m s^{-1}), and σ is the Boltzmann constant (1.38×10^{-23} J K^{-1}).

LST Downscaling Algorithm Based GWR Model

Geographical Weighted Regression (GWR) is one of the spatial regression techniques like ordinary least squares (Fotheringham et al., 2002). GWR is used to evaluate and examine the relationship between variables, taking into account the regression coefficients that vary according to geographical location. The GWR model is expressed as given in Eq. 10;

$$y_i = \beta_0(\mu_i, V_i) + \sum_{k=1}^{m} \beta_k(\mu_i, V_i)x_{ik} + \varepsilon_i \tag{10}$$

where y_i represents the dependent variable at location i, x_{ik}

Table 1 The LANDSAT 8 and MODIS land surface temperature (LST) data collected in this study

Season	Acquisition Time (MODIS LST Data)	Acquisition Time (LANDSAT 8 Data)
Winter	30.12.2020 07:35:00	30.12.2020 08:10:11
Spring	07.05.2021 07:35:00	07.05.2021 08:09:23
Summer	08.06.2021 07:35:00	08.06.2021 08:09:42
Autumn	14.10.2021 07:35:00	14.10.2021 08:10:19

represents the kth independent variable at location i, μ_i and V_i are the geographical coordinates of the ith location, $\beta_0(\mu_i, V_i)$ represents intercept, $\beta_k(\mu_i, V_i)$ represents kth slope of the regression model at location I, and ε_i is the regression residual at location i. β_0 and β_k parameters can be calculated from Eq. 11;

$$\hat{\beta}(\mu_i, V_i) = \left(X^T W(\mu_i, V_i)X\right)^{-1} X^T W(\mu_i, V_i)Y \quad (11)$$

where X and Y are matrices for independent and dependent variables, $W(\mu_i, V_i)$ is the weight matrix used to make observations close to a given point have larger weighted values, and $\hat{\beta}(\mu_i, V_i)$ presents estimated value of the regression coefficient β.

In this study, the GWR analysis was carried out using ArcGIS 10.8 software. NDVI and NDBI were chosen as auxiliary variables for LST downscaling. The NDVI was used to take into account the effects of different vegetation types on thermal processes at land surfaces. NDBI was used because it is accepted as an effective indicator of urban density. The flowchart of the GWR-based LST downscaling algorithm is shown in Fig. 3.

The first step in creating the GWR downscaling model, whose flowchart is given in Fig. 3, is to preprocess the LANDSAT 8 surface reflectance data. After preprocessing, NDVI and NDBI ancillary parameters were calculated using LANDSAT 8 data, and these indices were resampled as 1000 and 100 m, respectively. These resampled parameters were used to fit the relationship at coarse and fine resolution. The coarse resolution GWR model was created as in Eq. 12.

$$\begin{aligned} \text{LST}_i^{1000} = {}& \beta_0^{1000}(\mu_i, V_i) + \beta_1^{1000}(\mu_i, V_i)\text{NDVI}_i^{1000} \\ & + \beta_2^{1000}(\mu_i, V_i)\text{NDBI}_i^{1000} + \varepsilon_i^{1000} \end{aligned} \quad (12)$$

The intercept, coefficients and residuals obtained from the created coarse resolution GWR model were improved to 100 m spatial resolution using the kriging interpolation method. Finally, accepting that the temporal and spatial relationship between the LST and auxiliary variables is invariant depending on the scale, a model was created as in Eq. 13.

$$\begin{aligned} \text{LST}_i^{100} = {}& \beta_0^{100}(\mu_i, V_i) + \beta_1^{100}(\mu_i, V_i)\text{NDVI}_i^{100} \\ & + \beta_2^{1000}(\mu_i, V_i)\text{NDBI}_i^{100} + \varepsilon_i^{100} \end{aligned} \quad (13)$$

DisTrad Downscaling Method

Tested on US farmlands, this model was created with the aim of downscaling based on the inverse correlation between temperature and NDVI (Kustas et al., 2003). For this purpose, a second-order polynomial regression model was used (Eq. 14).

$$\widehat{\text{LST}} = a + b\text{NDVI} + c\text{NDVI}^2 \quad (14)$$

TsHARP Downscaling Method

The TsHARP model is a modification of the DisTrad algorithm (Agam et al., 2007). This method, which is the most widely used spatial downscaling model, uses the least-squares regression (OLS) function and NDVI is used as the predictive variable. The TsHARP model was created by testing on farmland in the USA. The TsHARP model is given in Eq. 15.

$$\widehat{\text{LST}} = a + b(1 - NDVI)^{0.625} \quad (15)$$

Performance Evaluation of Downscaling Models

The four statistical methods coefficient of determination (R^2), root-mean-square error-observations standard deviation ratio (RSR) and the Nash–Sutcliffe model efficiency coefficient (NSE) were used for the evaluation of models output against the observation station data.

The coefficient of determination is the ratio of how much of the variation in the observed data can be explained by the model. R^2 varies between 0 and 1; higher values indicate less error variation. Generally, values above 0.50 are considered acceptable (Wright, 1921; Santhi et al. 2001). The coefficient of determination is calculated by Eq. 16.

$$R^2 = \left(\frac{\sum_{i=1}^{n}(O_i - \overline{O}) \times (M_i - \overline{M})}{\sqrt{\sum_{i=1}^{n}(O_i - \overline{O})^2} \times \sqrt{\sum_{i=1}^{n}(M_i - \overline{M})^2}} \right)^2 \quad (16)$$

The RMSE (root of mean squared error) is one of the commonly used error index statistics (Chicco et al., 2021). It is generally accepted that the lower the RMSE, the better the model performance. However, the low value of this value varies according to the size of the values in the dataset. For this reason, RSR, which is a model evaluation statistic that will enable us to interpret these values more easily, has been developed (Singh et al., 2005). RSR converts the RMSE values to a standard value using the standard deviation values of the observations. It is calculated by dividing the RMSE and observation standard deviations (Eq. 17).

$$\text{RSR} = \frac{\sqrt{\sum_{i=1}^{n}|O_i - M_i|^2}}{\sqrt{\sum_{i=1}^{n}|O_i - \overline{O}|^2}} \quad (17)$$

The Nash–Sutcliffe efficiency coefficient gives a coefficient value that represents the predictive ability of the model. Its values range from $-\infty$ to 1. It is desired that the value it receives is between 0 and 1, and as it gets closer to 1, it shows that the model gives a good estimation result
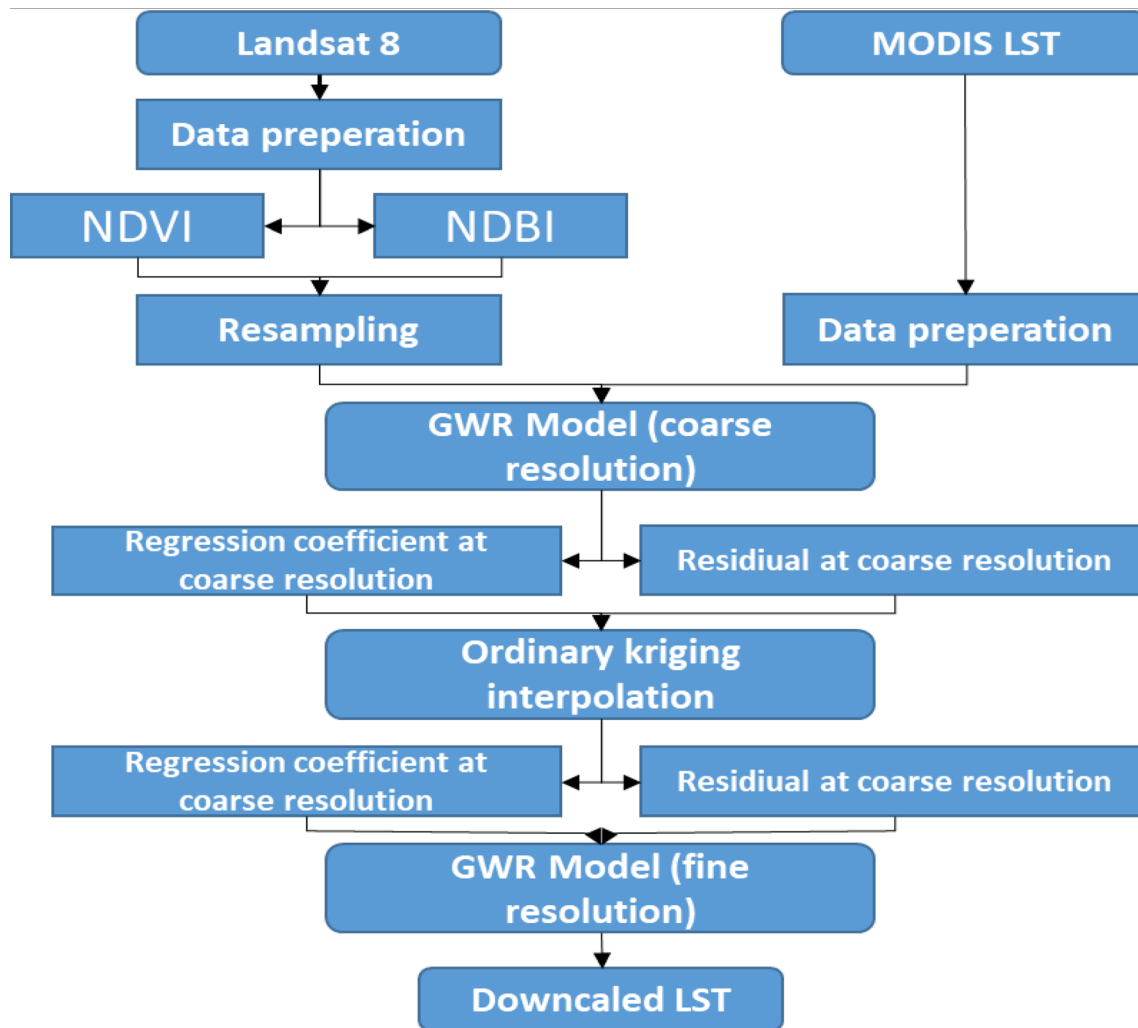
Fig. 3 Flowchart of the GWR-based LST downscaling algorithm

(Moriasi et al., 2007). NSE is calculated by the equation given below.

$$NSE = 1 - \frac{\sum_{i=1}^{n}(O_i - M_i)^2}{\sum_{i=1}^{n}(O_i - \overline{O})^2} \qquad (18)$$

In this equation, O_i is the observation station measurement, $\overline{O}$ is the average of the observation station measurements, M_i is the model output, $\overline{M}$ is the average of model output, and n is the number of data. RSR and NSE evaluation classes are given in Table 2.

Results and Discussion

Regression Analysis

The performances of the DisTrad, TsHARP and GWR models are compared and given in Fig. 4. High-resolution

Table 2 RSR and NSE performance evaluation table (Moriasi et al., 2007)

Degree	NSE	RSR
Very Good	0.75 − 1.00	0.00 − 0.50
Good	0.65 − 0.75	0.50 − 0.60
Satisfactory	0.50 − 0.65	0.60 − 0.70
Unsatisfactory	< 0.50	> 0.70

LST obtained from LANDSAT 8 data is often used as reference data in downscaling studies. In many studies, it has been explained that the relationship between MODIS LST and LANDSAT 8 LST is preferable in creating a downscaling model because of the low amount of error between them (RMSE < 2 °C).

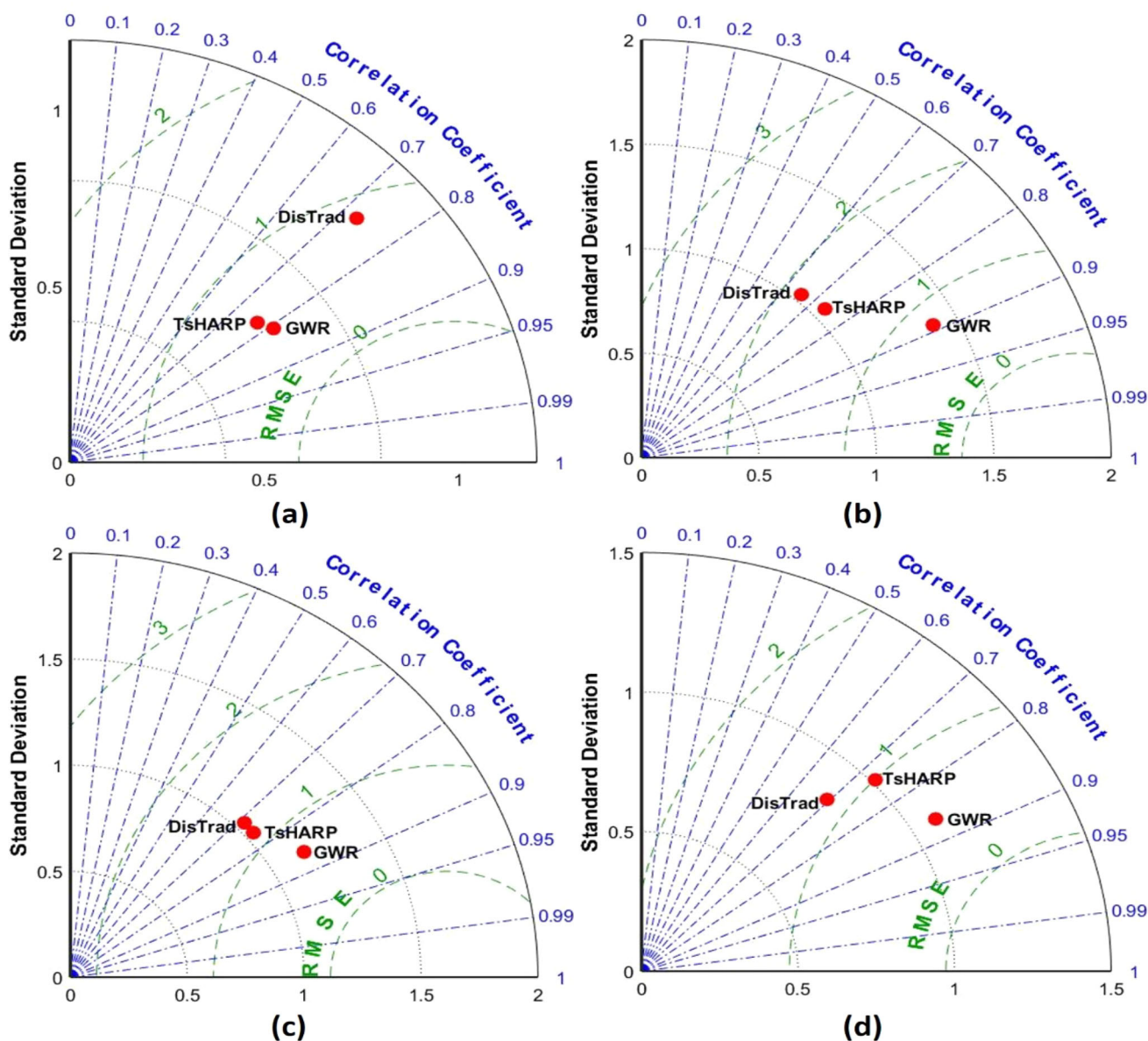For this reason, LANDSAT 8 LST which was obtained from LANDSAT 8 data was preferred as reference data in

Fig. 4 Taylor diagrams of downscaling models for **a** 30.12.2020, **b** 07.05.2021, **c** 08.06.2021, **d** 14.10.2021

this study. The correlation coefficient, standard deviations and RMSE values of the models are visualized with the Taylor diagram. When compared with other models, the correlation coefficient of the GWR-based model was higher than that of the other methods. In addition, it was determined that the prediction error of the GWR-based algorithm decreased significantly for all images (RMSE < 1). In conclusion, the statistical results show that considering the nonlinear relationship improves the accuracy of the downscaling results.

The spatial distribution pattern of the intersection, regression coefficients and residual values obtained by the kriging interpolation method of the GWR model is given in Fig. 5. When Fig. 5 is examined, it is seen that the spatial

distribution of these parameters is not homogeneous. Therefore, it has been determined that it is necessary to use spatially varying regression coefficients and residual values in order to model the relationship between LST and other auxiliary parameters. It has been understood that this is the most important reason why the GWR model achieved more successful results against the other two models. Duan and Li (2016) reported in their similar study that the GWR-based algorithm outperformed the TsHARP algorithm in terms of statistical results in the LST downscaling application. As a result of the statistical comparison, the RMSE value was calculated as 2.7 for the TsHARP algorithm and 2.3 for the GWR-based algorithm. In another similar study, Wang et al. (2021) calculated the RMSE performance as
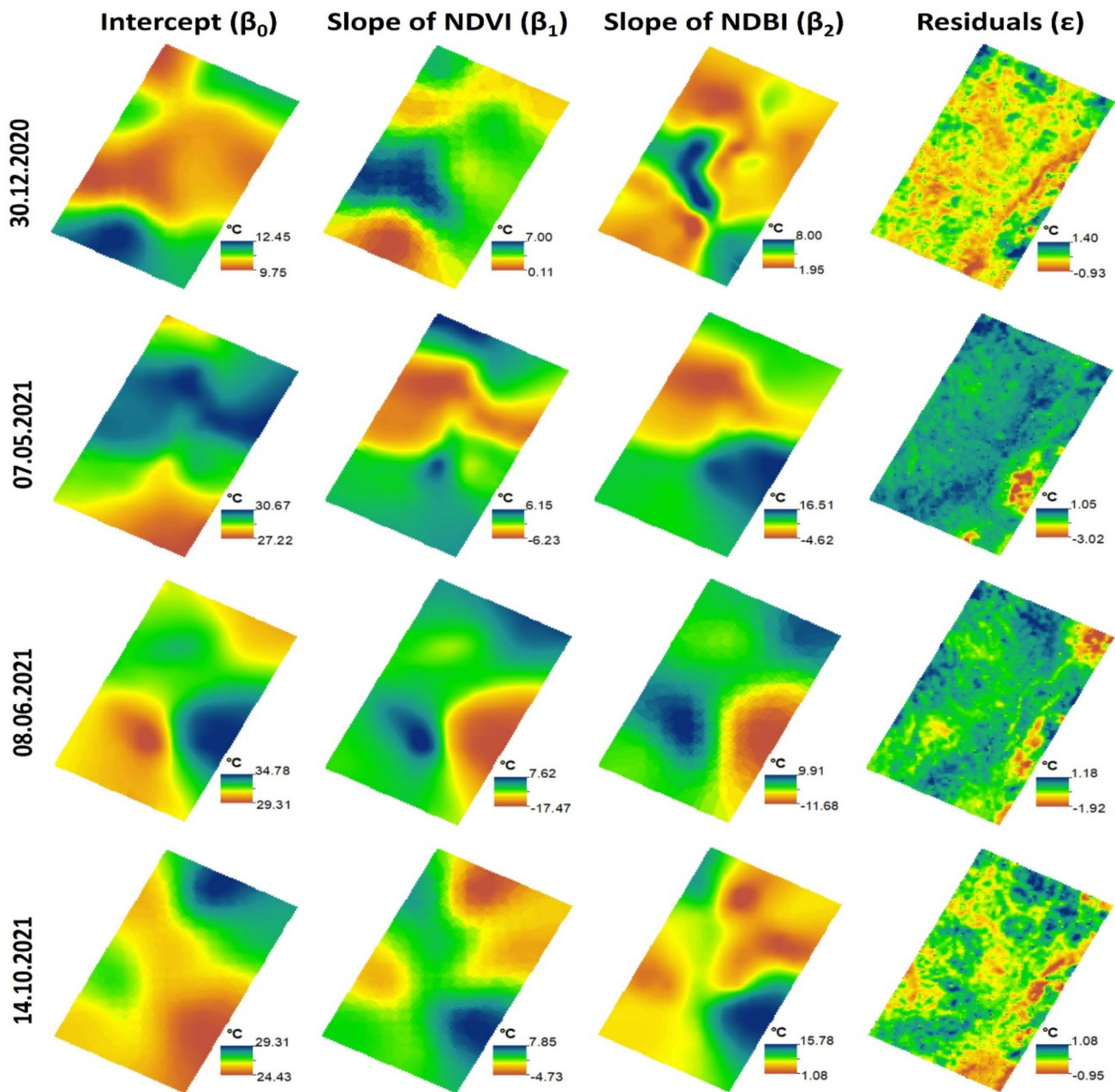
Fig. 5 Spatial distribution of kriging-interpolated regression coefficients and residuals for the GWR model in the study area

2.71 for the satellite image obtained for June of the GWR downscaling model and as 3.23 for the TsHARP algorithm.

Downscaling Results

Figure 6 shows the downscaling results obtained using different methods for a spatial resolution of 100 m. When the downscaling results are examined visually, it is seen that the downscaling model results are similar to the reference LANDSAT 8 LST. It is seen that the GWR model

obtained with the NDVI + NDBI parameters is the closest visually to the reference values among the models.

Additionally, it was observed that the TsHARP algorithm was better than the GWR algorithm for some areas. This is due to the smoothing effect of the GWR model, which can cause information loss. There are two important reasons for this effect. The first reason is that the interpolation methods applied in the process of obtaining images are based on the minimum mean square error method. Because of this method, low values are overestimated, while high values are underestimated.
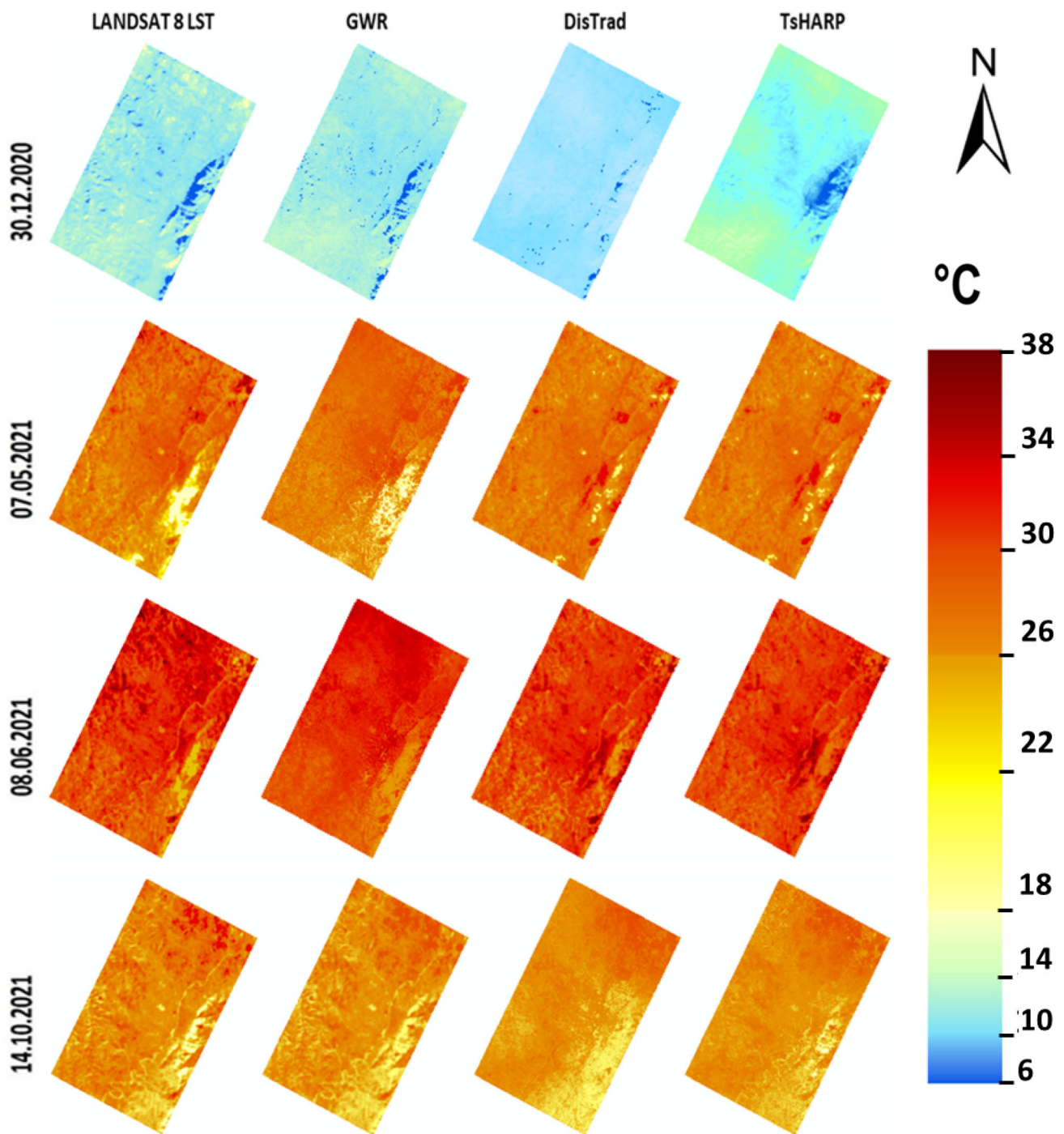
Fig. 6 Downscaling results at 100 m resolution obtained using different downscaling methods

Another reason is that in the process of resampling the auxiliary parameters NDBI and NDVI to 100 and 1000 m spatial resolution, the image becomes smoother than the original as a result of replacing the pixel values with the average values. As a result of this smoothness, some important information may be lost. However, because the GWR model takes into account the non-stationary relationship between LST and environmental factors, GWR outperformed the other two methods in terms of statistical results.

When the seasonal results for the GWR model are evaluated, it can be seen from Table 3 that the error amount is lower on the dates when the temperature is high, similar to the study of Wang et al. (2021). The lowest error amount was obtained for the image taken in the spring season (07.05.2021) (RSR = 0.48). The highest error rate was

Table 3 Performance evaluation of GWR downscaling model

Dates	RSR		NSE	
30.12.2020	0.61	Good	0.63	Satisfactory
07.05.2021	0.48	Very Good	0.77	Very Good
08.06.2021	0.53	Good	0.72	Good
14.10.2021	0.52	Good	0.73	Good

obtained for the image taken in winter (30.12.2020) (RSR = 0.61). Peng et al., (2019) evaluated the performance of the GWR downscaling model for September and October in another similar study conducted in Beijing, China. According to the results obtained, they calculated the RMSE values as 2.46 for September and 2.78 for October. When the calculated RSR values were examined, it was determined that the values obtained were within the acceptable threshold values given in the literature (RSR < 0.65). As for the model performance evaluation, it was determined that the estimations obtained were quite successful (NSE > 0.60). In general, it was determined that the downscaling model was more successful on hot and cloudless days compared to winter months. According to LULC (Fig. 2) map, results show that GWR downscaling model gave better accuracy in LST data in forestry and agricultural area than in urban area, because of using NDVI and NDBI indices.

Conclusion

This paper proposes a downscaling processing framework using the geographically weighted regression (GWR) model, which allows taking into account spatially heterogeneous relationships compared to commonly used predictive models. NDVI and NDBI data, which have a fine spatial resolution as auxiliary variables, were chosen for the LST downscaling model. A non-stationary relationship was established between these auxiliary variables and LST images using the GWR model. The accuracy of the GWR-based model was evaluated by comparing it with other commonly used models. GWR is a spatial downscaling method that has some advantages and disadvantages when compared to the TsHARP and DisTrad methods. GWR accounts for spatial autocorrelation, which allows to estimate local regression models, and considers the spatial variability of the data. GWR can be applied to linear and nonlinear relationships between variables. Also, GWR can be useful for downscaling of various environmental and meteorological variables such as precipitation, temperature, and wind speed. But GWR may be sensitive to

outliers, which could affect the accuracy of the model, and GWR is computationally intensive, which could be a limitation for some applications. Also, GWR's assumption of linearity may lead to an over- or underestimation of the relationships in certain cases.

The performance of the GWR-based algorithm was compared against that of the DisTrad and TsHARP algorithms using the concurrent LANDSAT 8 LST product as a reference LST dataset. A visual comparison of the spatial distribution of the downscaled LST results indicates that both the TsHARP and GWR-based algorithms outperform the DisTrad algorithm. Furthermore, a boxy artifact is observed in the TsHARP downscaled LST, whereas a smoothing effect occurs in the GWR-downscaled LST. When compared against the LANDSAT 8 reference LST dataset, the performance of the GWR-based algorithm is better than that of the TsHARP algorithm in terms of the statistical results.

We consider our study a successful attempt to build a nonlinear relationship in geographically weighted regressive algorithms where the downscaling result's accuracy is significantly improved due to the introduction of nonlinear terms. Data taken from different dates were investigated, and the proposed method gets better downscaling results in all datasets. The GWR model can be applied to urban areas. However, in extremely heterogeneous areas such as mountains, using nonlinear term in LST downscaling may introduce unstable results.

It is also recommended that before applying this algorithm to scenarios other than urban areas, the selection of more auxiliary parameters and optimization of their combination should be performed. For example, slope angle or incoming solar radiation may be more relevant in mountainous areas than NDBI. The overall procedure was repeatable, and the data are available for many different practices, thus providing a new urban heat island study tool.

Declarations

Conflict of Interest The authors declare no competing interests.

Ethics Approval The authors have agreed for authorship, read and approved the manuscript, and given consent for submission and subsequent publication of the manuscript.

Consent to Participate All authors consent to participate in the present study.

Consent for Publication All authors consent to participate in the present study.

References

Agam, N., Kustas, W. P., Anderson, M. C., Li, F., & Neale, C. M. U. (2007). A vegetation index based technique for spatial sharpening of thermal imagery. *Remote Sensing of Environment, 107*(4), 545–558. https://doi.org/10.1016/j.rse.2006.10.006

Alqasemi, A. S., Hereher, M. E., Al-Quraishi, A. M. F., Saibi, H., Aldahan, A., & Abuelgasim, A. (2020). Retrieval of monthly maximum and minimum air temperature using MODIS aqua land surface temperature data over the United Arab Emirates. *Geocarto International.* https://doi.org/10.1080/10106049.2020.1837261

Anderson, M. C., Kustas, W. P., Alfieri, J. G., Gao, F., Hain, C., Prueger, J. H., Evett, S., Colaizzi, P., Howell, T., & Chávez, J. L. (2012). Mapping daily evapotranspiration at LANDSAT spatial scales during the BEAREX'08 field campaign. *Advances in Water Resources, 50*, 162–177. https://doi.org/10.1016/j.advwatres.2012.06.005

Avdan, U., & Jovanovska, G. (2016). Algorithm for automated mapping of land surface temperature using LANDSAT 8 satellite data. *Journal of Sensors 2016.* https://doi.org/10.1155/2016/1480307

Badeck, F. W., Bondeau, A., Bottcher, K., Doktor, D., Lucht, W., Schaber, J., & Sitch, S. (2004). Responses of Spring Phenology to Climate Change. *The New Phytologist, 162*, 295–309. https://doi.org/10.1111/nph.2004.162.issue-2

Barsi, J. A., Schott, J. R., Hook, S. J., Raqueno, N. G., Markham, B. L., & Radocinski, R. (2014). LANDSAT-8 thermal infrared sensor (TIRS) vicarious radiometric calibration. *Remote Sens., 6*(11), 11607–11626. https://doi.org/10.3390/rs61111607

Bindhu, V. M., Narasimhan, B., & Sudheer, K. P. (2013). Development and verification of a non-linear disaggregation method (NL-DisTrad) to downscale MODIS land surface temperature to the spatial scale of LANDSAT thermal data to estimate evapotranspiration. *Remote Sensing of Environment, 135*, 118–129. https://doi.org/10.1016/j.rse.2013.03.023

Caihua, Y., Yonghong, L., Weijun, Q., Weidong, L., & Cheng, L. (2011). Application of urban thermal environment monitoring based on remote sensing in Beijing. *Procedia Environmental Sciences, 11*, 1424–1433. https://doi.org/10.1016/j.proenv.2011.12.214

Chicco, D., Warrens, M. J., & Jurman, G. (2021). The coefficient of determination R-squared is more informative than SMAPE, MAE, MAPE, MSE and RMSE in regression analysis evaluation. *PeerJ. Computer Science, 7*, e623. https://doi.org/10.7717/peerj-cs.623

Dominguez, A., Kleissl, J., Luvall, J. C., & Rickman, D. L. (2011). High-resolution urban thermal sharpener (HUTS). *Remote Sensing of Environment, 115*(7), 1772–1780. https://doi.org/10.1016/j.rse.2011.03.008

Duan, S. B., & Li, Z. L. (2016). Spatial downscaling of MODIS land surface temperatures using geographically weighted regression: Case study in Northern China. *IEEE Transactions on Geoscience and Remote Sensing, 54*(11), 6458–6469. https://doi.org/10.1109/TGRS.2016.2585198

Duan, S. B., Li, Z. L., Cheng, J., & Leng, P. (2017). Cross-satellite comparison of operational land surface temperature products derived from MODIS and ASTER data over bare soil surfaces. *ISPRS Journal of Photogrammetry and Remote Sensing, 126*, 1–10. https://doi.org/10.1016/j.isprsjprs.2017.02.003

Fotheringham, A. S., Brunsdon, C., & Charlton, M. E. (2002). *Geographically weighted regression: The analysis of spatially varying relationships* (p. 288). Wiley.

Hais, M., & Kucera, T. (2009). The influence of topography on the forest surface temperature retrieved from LANDSAT TM, ETM C and ASTER thermal channels. *ISPRS Journal of Photogrammetry and Remote Sensing, 64*, 585–591. https://doi.org/10.1016/j.isprsjprs.2009.04.003

Jeganathan, C., Hamm, N., Mukherjee, S., Atkinson, P. M., Raju, P., & Dadhwal, V. (2011). Evaluating a thermal image sharpening model over a mixed agricultural landscape in India. *Int J Appl Earth Obs., 13*(2), 178–191. https://doi.org/10.1016/j.jag.2010.11.001

Jiao, Z., Yan, G., Zhao, J., Wang, T., & Chen, L. (2015). Estimation of surface upward longwave radiation from MODIS and VIIRS clear-sky data in the Tibetan Plateau. *Remote Sensing of Environment, 162*, 221–237. https://doi.org/10.1016/j.rse.2015.02.021

Kustas, W. P., Norman, J. M., Anderson, M. C., & French, A. N. (2003). Estimating subpixel surface temperatures and energy fluxes from the vegetation index—Radiometric temperature relationship. *Remote Sensing of Environment, 85*(4), 429–440. https://doi.org/10.1016/S0034-4257(03)00036-1

Merlin, O., Duchemin, B., Hagolle, O., Jacob, F., Coudert, B., Chehbouni, G., Dedieu, G., Garatuza, J., & Kerr, Y. (2010). Disaggregation of MODIS surface temperature over an agricultural area using a time series of Formosat-2 images. *Remote Sensing of Environment, 114*(11), 2500–2512. https://doi.org/10.1016/j.rse.2010.05.025

Moriasi, D. N., Arnold, J. G., Van Liew, M. V., Bingner, R. L., Harmel, R. D., & Veith, T. L. (2007). Model evaluation guidelines for systematic quantification of accuracy in watershed simulations. *Transactions of the ASABE, 50*(3), 885–900. https://doi.org/10.13031/2013.23153

Peng, Y. D., Li, W. S., Luo, X. B., & Li, H. (2019). A geographically and temporally weighted regression model for spatial downscaling of MODIS land surface temperatures over urban heterogeneous regions. *IEEE T Geosci Remote, 57*, 5012–5027. https://doi.org/10.1109/TGRS.2019.2895351

Purevdorj, T. S., Tateishi, R., Ishiyama, T., & Honda, Y. (1998). Relationships between percent vegetation cover and vegetation indices. *International Journal of Remote Sensing, 19*, 3519–3535. https://doi.org/10.1080/014311698213795

Rawat, K. S., Sehgal, V. K., & Ray, S. S. (2019). Downscaling of MODIS thermal imagery. *The Egyptian Journal of Remote Sensing and Space Sciences, 22*, 49–58. https://doi.org/10.1016/j.ejrs.2018.01.001

Singh, J., Knapp, H. V., Arnold, J. G., & Demissie, M. (2005). Hydrologic modeling of the Iroquois River watershed using HSPF and SWAT. *Journal of the American Water Resources Association, 41*(2), 361–375. https://doi.org/10.1111/j.1752-1688.2005.tb03740.x

Song, W., Mu, X., Ruan, G., Gao, Z., Li, L., & Yan, G. (2017). Estimating fractional vegetation cover and the vegetation index of bare soil and highly dense vegetation with a physically based method. *International Journal of Applied Earth Observation and*

Geoinformation, 58, 168–176. https://doi.org/10.1016/j.jag.2017.01.015

Sun, Z., Wang, Q., Ouyang, Z., Watanabe, M., Matsushita, B., & Fukushima, T. (2007). Evaluation of MOD16 algorithm using MODIS and ground observational data in winter wheat field in North China Plain. *Hydrological Processes, 21*, 1196–1206. https://doi.org/10.1002/hyp.6679

Wang, S., Luo, Y., Li, X., Yang, K., Liu, Q., Luo, X., & Li, X. (2021). Downscaling land surface temperature based on non-linear geographically weighted regressive model over urban areas. *Remote. Sens., 13*, 1580. https://doi.org/10.3390/rs13081580

Wright, S. (1921). Correlation and causation. *Journal of Agricultural Research, 20*, 557–585.

Wu, P., Shen, H., Zhang, L., & Göttsche, F. M. (2015). Integrated fusion of multi-scale polar-orbiting and geostationary satellite observations for the mapping of high spatial and temporal resolution land surface temperature. *Remote Sensing of Environment, 156*, 169–181. https://doi.org/10.1016/j.rse.2014.09.013

Wu, P., Shen, H., Zhang, L., & Göttsche, F. M. (2015). Integrated fusion of multi-scale polar-orbiting and geostationary satellite observations for the mapping of high spatial and temporal resolution land surface temperature. *Remote Sensing of Environment, 156*, 169–181. https://doi.org/10.1016/j.rse.2014.09.013

Yang, G., Pu, R., Huang, W., Wang, J., & Zhao, C. (2010). A novel method to estimate subpixel temperature by fusing solar-reflective and thermal infrared remote-sensing data with an artificial neural network. *IEEE Transactions on Geoscience and Remote Sensing, 48*(4), 2170–2178. https://doi.org/10.1109/TGRS.2009.2033180

Yang, G., Pu, R., Zhao, C., Huang, W., & Wang, J. (2011). Estimation of subpixel land surface temperature using an endmember index based technique: A case examination on ASTER and MODIS temperature products over a heterogeneous area. *Remote Sensing of Environment, 115*(5), 1202–1219. https://doi.org/10.1016/j.rse.2011.01.004

Zareie, S., Khosravi, H., & Nasiri, A. (2016). Derivation of land surface temperature from LANDSAT thematic mapper (TM) sensor data and analyzing relation between land use changes and surface temperature. Solid Earth Discussions. https://doi.org/10.5194/se-2016-22

Zha, Y., Gao, J., & Ni, S. (2003). Use of normalized difference built-up index in automatically mapping urban areas from TM imagery. *International Journal of Remote Sensing, 24*(3), 583–594. https://doi.org/10.1080/01431160304987